

Isolating vector boson scattering at the CERN LHC: Gauge cancellations and the equivalent vector boson approximation versus complete calculations

Elena Accomando,^{*} Alessandro Ballestrero,[†] Aissa Belhouari,[‡] and Ezio Maina[§]

INFN, Sezione di Torino and Dipartimento di Fisica Teorica, Università di Torino, Via Giuria 1, 10125 Torino, Italy
(Received 18 August 2006; published 20 October 2006)

We have studied the possibility of extracting the $W^+W^- \rightarrow W^+W^-$ signal using the process $us \rightarrow cdW^+W^-$ as a test case. We have investigated numerically the strong gauge cancellations between signal and irreducible background, critically analyzing the reliability of the equivalent vector boson approximation which is commonly used to define the signal. Complete matrix elements are necessary to study electroweak symmetry breaking effects at high WW invariant mass.

DOI: [10.1103/PhysRevD.74.073010](https://doi.org/10.1103/PhysRevD.74.073010)

PACS numbers: 12.15.-y

I. INTRODUCTION

The mechanism of electroweak symmetry breaking (EWSB) will be one of the primary topics to be investigated at the CERN LHC, both through direct searches for the Higgs boson and careful analysis of boson-boson scattering processes. Detailed reviews and extensive bibliographies can be found in Refs. [1–3]. The nature of the interaction between longitudinally polarized vector bosons is strongly related to the Higgs mass, or possibly to the absence of the Higgs particle. If a relatively light Higgs exists, then the V_L 's are weakly coupled, while they are strongly interacting if the Higgs mass is large or the Higgs is nonexistent [4].

It should be noted that the Goldstone theorem and the Higgs mechanism do not require the existence of elementary scalars. It is conceivable and widely discussed in the literature that bound states are responsible for EWSB.

At the LHC no beam of on-shell EW vector bosons will be available. Incoming quarks will emit spacelike virtual bosons which will then scatter among themselves and finally decay. These processes have been scrutinized for a long time in order to uncover the details of the EWSB mechanism in this realistic setting [5–7]. Naively one expects that at large boson-boson invariant masses, the diagrams containing vector boson fusion subdiagrams should dominate the total cross section while the off-shellness of the bosons initiating the scattering process should become less and less relevant. Together with the keen interest for Higgs production in vector boson fusion, this has led to the development of the equivalent vector boson approximation (EVBA) [8–10]. The EVBA provides a particularly simple and appealing framework in which the cross section for the full process is approximated by the convolution of the cross section for the scattering of on-shell vector bosons times appropriate distribution functions

which can be interpreted as the probability of the initial state quarks to emit the EW bosons which then interact.

This approach relies on the neglect of all diagrams which do not include boson-boson scattering subdiagrams and on a suitable on-shell projection for the scattering set of diagrams. Since the approximate boson-boson interaction is expressed in terms of on-shell particles, it is straightforward to separate the different boson polarizations. It is well known that the set of scattering diagrams is not separately gauge invariant, while both the on-shell amplitude and the distribution functions which appear in the EVBA are gauge independent.

In [11] it has been shown that when vector bosons are allowed to be off mass shell in boson-boson scattering, the amplitude grows faster with energy compared with the amplitude for on-shell vectors. Subsequently, it has been pointed out in [12] that the problem of bad high energy behavior of WW scattering diagrams can be avoided by the use of the axial gauge. Recently WZ production at the LHC [13] has been analyzed in axial gauge with very encouraging results. It should be noted that the results in [12] have been obtained under the assumption that the transverse momenta of the produced W 's are of the order of the Higgs mass and that each is much larger than the W mass. It is therefore not obvious to what degree the conclusions of Ref. [12] can be applied in the LHC environment, particularly for light Higgs masses as preferred by global standard model (SM) fits.

The EVBA has some undesirable features: a number of unphysical cuts need to be introduced to tame the singularities generated by the on-shell projection, which are absent from the exact amplitude. In the literature, a number of comparisons of exact and EVBA calculations have appeared with conflicting results [7,14,15].

For these reasons, in the present paper we have critically examined the role of gauge invariance in VV fusion processes and the reliability of the EVBA in describing them. We would like to determine regions in phase space, at least in a suitable gauge, which are dominated by the scattering set of diagrams.

^{*}Electronic address: accomand@to.infn.it

[†]Electronic address: ballestr@to.infn.it

[‡]Electronic address: belhouar@to.infn.it

[§]Electronic address: maina@to.infn.it

If this was the case, then it would be possible to employ this set of diagrams to define a “signal,” that is, a pseudo-variable which could be used to compare the results from the different collaborations. The signal is not necessarily directly observable but it should be possible to relate it via Monte Carlo predictions to measurable quantities. If such a definition is to be useful, it must correspond as closely as possible to the process which needs to be studied, and the Monte Carlo corrections must be small. If instead, as we are led to believe by the results shown in the following, the VV scattering diagrams do not constitute the dominant contribution in any gauge or phase space region, there is no substitute for the complete amplitude for studying boson fusion processes at the LHC. We cannot claim to have examined all possible gauge schemes; however, we have studied the most commonly used ξ -type gauges and the implementation of the axial gauge proposed in [12]. The results obtained with the full amplitude show that the mechanism of EWSB can indeed be investigated even without separating out the scattering set of diagrams.

II. VV SCATTERING AND GAUGE INVARIANCE

In order to study the implications of gauge invariance in VV fusion processes, we have concentrated on the specific process $us \rightarrow cdW^+W^-$ in proton-proton collisions at the LHC. The corresponding Feynman diagrams can be classified in two different sets (Fig. 1), the boson-boson fusion one [Fig. 1(a)] and all the rest [Fig. 1(b)] in which at least one final W is emitted by a fermion line. The two sets are not separately gauge invariant. We have started our analysis from the contribution of the boson-boson fusion diagrams and their interference with the remaining ones. We have considered the unitary, Feynman, and Landau gauges. Among these, we find that the Feynman gauge is the one which minimizes the cancellations between set (a) of Fig. 1 and the nonscattering diagrams. We have also performed the calculation in the axial gauge $n_\mu A^\mu = 0$ within the scheme proposed in Ref. [12]. In the Appendix we have collected the main corresponding Feynman rules. We have tried different n_μ gauge vectors and we find that the choice

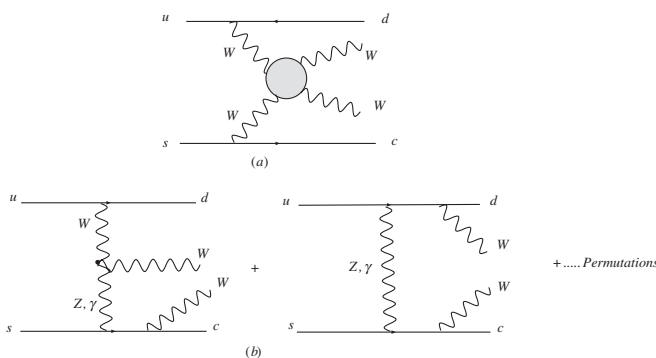


FIG. 1. Main diagram topologies for the process $us \rightarrow cdW^+W^-$.

$n_\mu = (1, 0, 0, 1)$ (the incoming protons propagate along the z axis) is the best one. For brevity we will refer to this framework as axial gauge in the following. We present results for the unitary, Feynman, and axial gauges, showing the contribution of all diagrams (all) and of the WW scattering diagrams (WW), together with their ratio WW/all . When this ratio is significantly greater than 1, the contribution of nonscattering diagrams is of the same order as the contribution of the WW scattering ones and important cancellations take place between the two sets.

In Table I the total cross sections and their ratios are computed in the limit of infinite Higgs mass. This limit will also be referred to in the following as the no-Higgs case. We find that the axial gauge is the one in which the interferences are the least severe with a ratio of about 2, while the ratios for the unitary and Feynman gauges are 358 and 13, respectively. The inclusion of a light Higgs ($M_h = 200$ GeV) does not improve matters: on the contrary, the ratios become even larger as shown in Table II for $M_h = 200$ GeV, doubling for the unitary and Feynman gauges.

The comparison of total cross sections is only a preliminary step. It provides the general behavior but it cannot give information on the different regions of phase space. For this reason we have evaluated the distribution of different kinematical variables with the goal of finding regions where the interferences are not important. If such regions exist it will be possible to define a set of cuts which allow the extraction of the WW scattering amplitude. Figure 2 shows the distributions of the diboson invariant mass for the complete set of diagrams and for the WW diagrams

TABLE I. WW diagrams and complete set of diagram cross sections and their ratios computed in different gauges without Higgs contribution. We have used the CTEQ5 pdf set with scale M_W .

	σ (pb) all diagrams	σ (pb) WW diagrams	Ratio of WW/all diagrams
Unitary gauge	1.86×10^{-2}	6.67	358
Feynman gauge	1.86×10^{-2}	0.245	13
Axial gauge	1.86×10^{-2}	3.71×10^{-2}	2

TABLE II. WW diagrams and complete set of diagram cross sections and their ratios computed in different gauges with a $M_h = 200$ GeV Higgs and $M(WW) > 300$ GeV.

	σ (pb) all diagrams	σ (pb) WW diagrams	Ratio of WW/all diagrams
Unitary gauge	8.50×10^{-3}	6.5	765
Feynman gauge	8.50×10^{-3}	0.221	26
Axial gauge	8.50×10^{-3}	2.0×10^{-2}	2.3

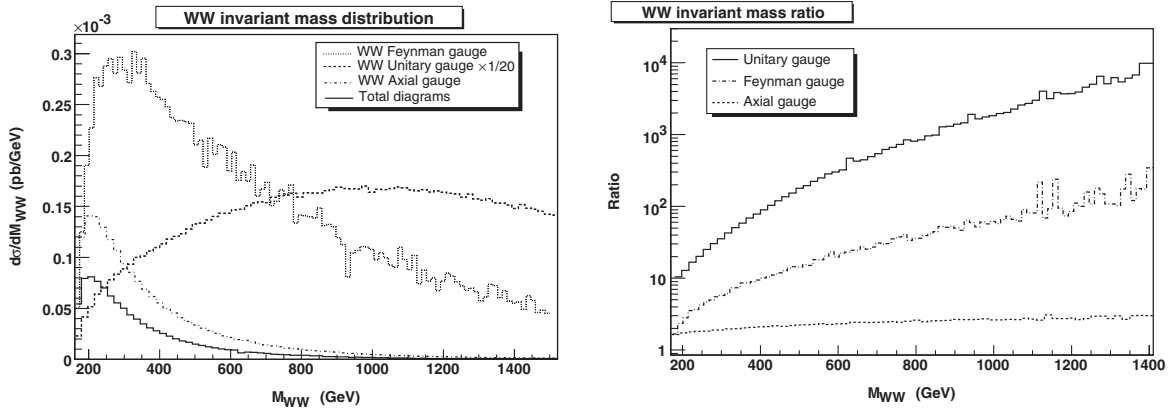


FIG. 2. Distribution of $d\sigma/dM_{WW}$ for the process $PP \rightarrow us \rightarrow cdW^+W^-$ for all diagrams, WW diagrams, and their ratio in unitary, Feynman, and axial gauges in the infinite Higgs mass limit. The unitary gauge data in the left-hand plot have been divided by 20 for better presentation.

only, together with the ratio $(d\sigma(WW)/dM)/(d\sigma(\text{all})/dM)$. We have chosen the vector boson pair invariant mass distribution as a prototype but the same conclusions are reached with all other variables. The results of Fig. 2 have been obtained for a very large Higgs mass but the general behavior is not modified by the inclusion of a light Higgs. The distributions obtained with the full set of diagrams and with the WW fusion set only are quite different in the unitary and Feynman gauges. The ratio is also large over the whole interval and especially in the region of high invariant mass which is the most important one for EWSB studies. Again, the axial gauge gives the best result, with distributions which have the same general shape in the two cases. The ratio in this gauge remains, however, greater than 2, apart from a very small region at low invariant mass.

We have completed our study by analyzing bidimensional distributions of several pairs of kinematical variables. These double distributions allow us to analyze, in particular, the situation where the two incoming bosons have small virtualities ($t_{1,2} \rightarrow 0$). In this region the WW scattering diagrams are expected to dominate. The same behavior found previously is observed: the effect of the interferences is much more relevant in the unitary gauge with respect to the others. In general, the WW fusion subset has a different behavior compared with the complete calculation. In Fig. 3 we report $d\sigma/dt_1 dt_2$ in the axial gauge where $t_{1,2} = \sqrt{-(p_{u,s} - p_{d,c})^2}$ are the square root of the absolute value of the invariant masses of the incoming off-shell W 's. The corresponding ratio distributions [plots (c), (d)] show that, even in the limited region $0 < t_{1,2} < 250$ GeV, the WW contribution alone does not provide a realistic description of the complete set of diagrams. Even in the axial gauge significant cancellations take place. The ratio is highly asymmetric in the t_1 - t_2 plane, reflecting its sensitivity to the choice of the axial gauge axis (recall that in this case the gauge vector is along the z axis) and WW scattering diagrams alone provide only a very rough esti-

mate of the cross section. It is, however, possible to find regions, typically for $t_{1,2} > 200$ GeV where the cross section is greatly reduced, where the ratio of the two results is around 1. For comparison we also show the distributions obtained from the WW fusion subset in the unitary (e) and Feynman (f) gauges. Their shape and normalization are completely different from the results obtained from the full amplitude.

From this sample of results one can conclude that the WW scattering diagrams do not constitute the dominant contribution in any phase space region for the gauges we have examined. For the axial gauge, which in various cases shows ratios of order 2, we remark that these have been obtained only with a particular timelike gauge vector $n_\mu = (1, 0, 0, 1)$. For any other spacelike n_μ , the interferences are so important that even the numerical integration becomes difficult for the set of WW diagrams whereas no problem occurs for the full set of diagrams. So we did not succeed in finding a gauge vector of the type suggested in [12] for which the cancellations are negligible. Even with our best choice of n_μ , the distributions of the different kinematical variables show the presence of large interferences between the two subsets of diagrams over most of phase space, indicating that the WW diagrams are not dominating. As a consequence a question mark is put on the possibility to isolate the WW scattering contribution by restricting the calculations to the corresponding diagrams. The reliability of approximation methods based on such an approach then becomes suspicious. For this reason we have completed our analysis by studying the effective vector boson approximation applied to our prototype process.

III. THE EFFECTIVE VECTOR BOSON APPROXIMATION

The effective photon approximation, known also as the Weizsäcker-Williams approximation [16,17], has proved to be a useful tool in the study of photon-photon processes

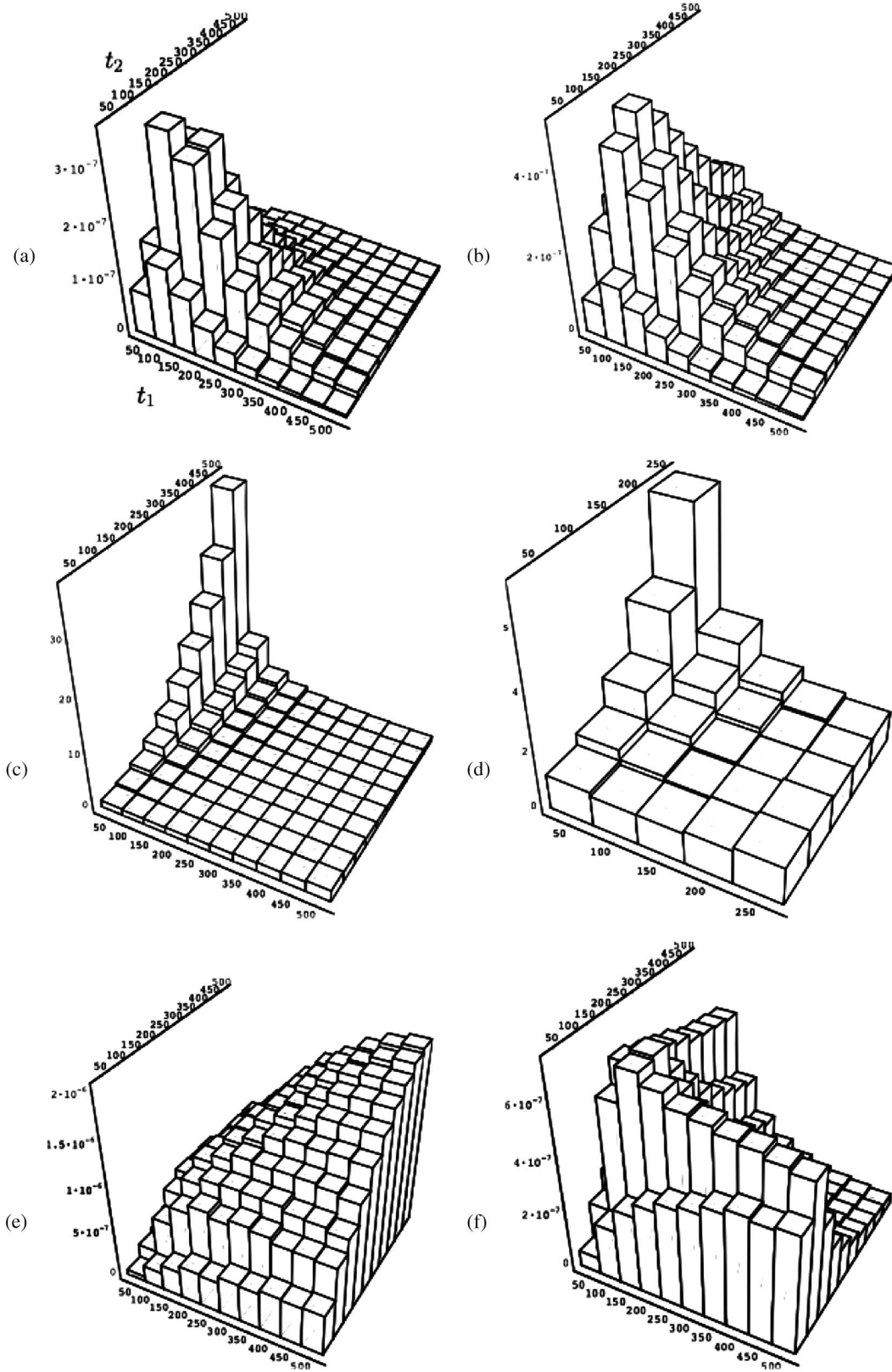


FIG. 3. Double differential distributions of $d\sigma/dt_1 dt_2$ (pb/GeV²) with $t_{1,2} = \sqrt{-(p_{u,s} - p_{d,c})^2}$ for the process $PP \rightarrow us \rightarrow dcW^+W^-$, using all diagrams (a) or only the WW fusion subset in axial gauge (b). The two plots in the central row represent the ratio WW /all in the axial gauge as a function of t_1, t_2 for the total region (c) and for small t 's (d). For comparison we also show the distributions of the WW fusion subset in the unitary (e) and Feynman (f) gauges. All invariants are in GeV.

at e^+e^- colliders. Encouraged by this success the approach has been extended to processes involving massive vector bosons [8–10] under the name of the effective vector boson approximation. The EVBA was first applied at hadron colliders in connection with Higgs production $pp \rightarrow H + X$ [18] and subsequently to vector boson processes of the type $pp \rightarrow (H \rightarrow V_3V_4) + X \rightarrow V_3V_4 + X$ [7,19] in order to obtain EVBA predictions for the production of a vector boson pair not necessarily near the Higgs resonance and to study the strongly interacting scenario.

In analogy to the QED case, the application of EVBA to these processes consists of the following:

- (1) Restricting the computation to the vector boson scattering diagrams, neglecting diagrams of bremsstrahlung type.
- (2) Projecting on shell the momenta of the vector bosons which take part in the scattering: $q_{1,2}^2 = M_{V_{1,2}}^2$. Here it is important to notice that, contrary to the $\gamma\gamma$ processes where the photon momentum can reach the on-shell value $q_{1,2}^2 = 0$, for the massive vector bosons the on-shell point $q_{1,2}^2 = M_{V_{1,2}}^2$ is outside the accessible phase space region $q_{1,2}^2 \leq 0$.
- (3) Approximating the total cross section of the process $f_1f_2 \rightarrow f_3f_4V_3V_4$ as the convolution of the vector boson luminosities $\mathcal{L}_{\text{Pol}_1\text{Pol}_2}^{V_1V_2}(x)$ with the on-shell vector boson scattering cross section:

$$\begin{aligned} & \sigma(f_1f_2 \rightarrow f_3f_4V_3V_4) \\ &= \int \sum_{V_1, V_2} \sum_{\text{Pol}_1, \text{Pol}_2} \mathcal{L}_{\text{Pol}_1\text{Pol}_2}^{V_1V_2}(x) \sigma_{\text{Pol}}^{\text{on}}(V_1V_2 \\ & \rightarrow V_3V_4, xs_{qq}) dx. \end{aligned} \quad (1)$$

Here $x = M(V_1V_2)^2/s_{qq}$, while $M(V_1V_2)$ is the vector boson pair invariant mass and s_{qq} is the partonic center-of-mass (CM) energy.

It is clear that this approximation provides a simplification from the computational point of view and can exploit the properties of on-shell boson-boson scattering. In first applications of EVBA to vector boson scattering, further approximations have been adopted. The zero angle scattering approximation has been used for the process $V_1V_2 \rightarrow V_3V_4$ so the transverse momentum of the incoming bosons has been neglected. The zero mass limit for the vector boson mass $M_V \rightarrow 0$ has also been considered in the computation of the luminosity. In this early application of EVBA, only the contribution from longitudinal modes was considered, while the contribution from transverse states was neglected. The EVBA results depended strongly on the details of the approximations made. The EVBA generally overestimated the complete perturbative calculation, in some cases by a factor of 3 [20]. Progressively, more refined and rigorous formulations of EVBA have been proposed, avoiding as much as possible the mentioned approximations. In the implementation of Ref. [21] no

kinematical approximations are used and all vector boson polarization states as well as their interferences are taken into account. Inspired by the strategy of [21], we have further improved the EVBA. We have used an approach where not only are all kinematic approximations avoided, but also the luminosity computation is not needed. This allows us, in particular, to keep all final particle properties (momenta, angles, ...) as they would be in an exact calculation, contrary to the traditional approach where a preintegration is performed to obtain the vector boson luminosities.

IV. EVBA APPLICATION TO THE $PP \rightarrow us \rightarrow dcW^+W^-$ PROCESS

In [21] a precise formulation of EVBA has been developed. It is based on a factorization technique for analyzing Feynman diagrams which leads to exact probability distribution functions for the vector bosons [22]. This improved formulation does not invoke any kinematical approximation such as those mentioned in the previous paragraph. The only approximation concerns the on-shell continuation of the vector boson scattering cross section. Using this factorization technique and the relation between the polarization vectors and the vector boson propagator in unitary gauge, the matrix element for any process of the kind $f_1f_2 \rightarrow f_3f_4 + Y$, where Y is produced by vector boson fusion, can be written as

$$\begin{aligned} M &= e^2 \sum_{m,n=-1}^1 (-1)^{m+n} \frac{j_1(p_1, p_3) \cdot \epsilon_1^*(m)}{q_1^2 - M_{V_1}^2} \\ & \times \frac{j_2(p_2, p_4) \cdot \epsilon_2^*(n)}{q_2^2 - M_{V_2}^2} \times M(m, n). \end{aligned} \quad (2)$$

$q_{1,2}$ are the momenta of the initial vector bosons; $\epsilon_j(m)$ are their polarization vectors corresponding to the different helicity states $m = 0, \pm 1$. We have used the same expressions, conventions, and frame to define them as given in [21]. They are normalized according to

$$\epsilon_j(m) \cdot \epsilon_j^*(m') = \delta_{m,m'} (-1)^m \quad (3)$$

and satisfy the completeness relation

$$\sum_{m=-1,0,1} \epsilon_j^\mu(m) \epsilon_j^{*\nu}(m) = -g^{\mu\nu} + \frac{q_j^\mu q_j^\nu}{M_{V_j}^2}. \quad (4)$$

$j_{1,2}$ are the quark currents and $M(m, n)$ the off-shell scattering amplitude of the vector boson subprocess $V_1V_2 \rightarrow V_3V_4$:

$$M(m, n) = \sum_{\mu\nu\alpha\beta} \epsilon_1^\mu(m) \epsilon_2^\nu(n) T_{\mu\nu\alpha\beta} \epsilon_3^{*\alpha} \epsilon_4^{*\beta}. \quad (5)$$

Usually an integration is performed over all the integration variables which are not concerned with the vector boson scattering subprocess as a first step to compute the vector boson luminosities. Denoting these variables by

$\{\phi\}$, one can write the total cross section expression as

$$\sigma_{\text{tot}} = \int g(q_1^2, q_2^2, x, \phi) d\phi \sigma_{\text{off}}^{VV}(W^2, q_1^2, q_2^2) dq_1^2 dq_2^2 dx. \quad (6)$$

$g(q_1^2, q_2^2, x, \phi)$ represents all terms which are independent of the vector boson scattering subprocess. Here $x = \frac{W^2}{s_{qq}}$, where $W^2 = (q_1 + q_2)^2$ is the diboson invariant mass squared.

$$\sigma_{\text{off}}^{VV}(W^2, q_1^2, q_2^2) \sim \int \sum_{m,n,m',n'} M(m,n) M^*(m',n') dp_V \quad (7)$$

is the off-shell $VV \rightarrow VV$ cross section and dp_V the final state vector boson phase space element. The next step is the extrapolation to on-shell masses. In [21] it is achieved by simple proportionality factors between the off-shell and on-shell cross sections:

$$\sigma_{\text{Pol}}^{\text{off}}(W^2, q_1^2, q_2^2) = f_{\text{Pol}}(W^2, q_1^2, q_2^2) \sigma_{\text{Pol}}^{\text{on}}(W^2, M_{V_1}^2, M_{V_2}^2). \quad (8)$$

The subscript Pol refers to the different vector boson polarization states, and M_{V_1} , M_{V_2} to the masses of the vector bosons initiating the scattering process. While we refer to [21] for the details, we reproduce here the form factor f_{Pol} expression according to the different polarization configurations:

$$f_{TT} = 1, \quad f_{LL} = \left(\frac{M_{V_1}^2}{-q_1^2} \right) \left(\frac{M_{V_2}^2}{-q_2^2} \right), \quad (9)$$

$$f_{LT} = \left(\frac{M_{V_1}^2}{-q_1^2} \right), \quad f_{TL} = \left(\frac{M_{V_2}^2}{-q_2^2} \right), \quad (10)$$

$$f_{TLTL} = \left(\frac{M_{V_1}^2}{\sqrt{-q_1^2}} \right) \left(\frac{M_{V_2}^2}{\sqrt{-q_2^2}} \right). \quad (11)$$

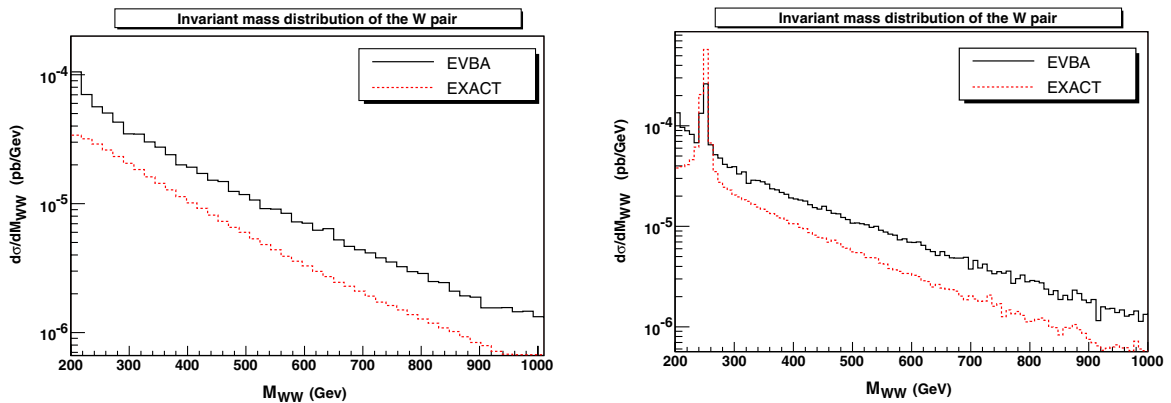


FIG. 4 (color online). WW invariant mass distribution $M(WW)$ for the process $us \rightarrow dcW^+W^-$ with EVBA (black solid curve) and with exact complete computation (red dashed curve) for the infinite Higgs mass case (left panel) and $M_h = 250$ GeV (right panel) at the LHC.

Finally one can write the cross section expression in the EVBA approximation as

$$\sigma_{\text{tot}}^{\text{EVBA}} = \int g(q_1^2, q_2^2, x, \phi) d\phi dq_1^2 dq_2^2 \sum_{\text{Pol}_1 \text{Pol}_2} f_{\text{Pol}} \sigma_{\text{Pol}}^{\text{on}} dx. \quad (12)$$

By comparison with Eq. (1) the luminosity can be expressed as

$$\mathcal{L}_{\text{Pol}_1 \text{Pol}_2}^{WW}(x) = \int g(q_1^2, q_2^2, x, \phi) f_{\text{Pol}} d\phi dq_1^2 dq_2^2. \quad (13)$$

In our implementation we have used the same assumptions but we have performed the on-shell extrapolation at the matrix element level. This allows us to keep all the terms $M(m,n)M^*(m',n')$ ($m \neq m', n \neq n'$) in the total amplitude squared. The off-shell vector boson scattering matrix element $M(m,n)$ in (2) and (5) is expressed in terms of the corresponding on-shell matrix elements and the polarization factors (9) as

$$M(m,n) = \sqrt{f_{mn}} M^{\text{on}}(m,n) \quad (m,n = L,T). \quad (14)$$

Moreover, we have not employed any luminosity function but we have used the diagrammatical expression of the fermion lines, evaluating them for each kinematical configuration and polarization.

V. COMPARISON BETWEEN EVBA AND EXACT RESULTS

We have computed the total cross section and the distribution of the vector boson pair invariant mass $M(WW)$ with an exact calculation and in EVBA for the process $PP \rightarrow us \rightarrow cdW^+W^-$ at the LHC. Cuts are necessary in EVBA to avoid the photon t channel propagator pole and the form factor (9) ($q_1^2 \rightarrow 0, q_2^2 \rightarrow 0$) singularities. We have restricted the CM scattering angle of the W 's and the

laboratory frame polar angle of the c and d quarks in order to deal with photon and form factor singularities, respectively. For comparison purposes, the same cuts have also been applied in the exact calculation even though no singularity appears in this case. Unless otherwise noted, we have used a cut of 10 degrees for all three angles.

For the total cross section in the no-Higgs case we obtain 0.63×10^{-2} pb with an exact calculation and 1.36×10^{-2} pb in EVBA. For $M_h = 250$ GeV we obtain 1.32×10^{-2} pb and 1.64×10^{-2} pb, respectively. The corresponding distributions of the WW invariant mass are shown Fig. 4. The EVBA overestimates the exact calculation by a factor of about 2, which is almost insensitive to $M(WW)$, with the exception of the Higgs peak region at $M_h = 250$ GeV where the exact result is larger than the EVBA one.

We have checked our implementation of the EVBA against the one used in PYTHIA for the scattering of longitudinally polarized W 's. The two results are only in qualitative agreement as expected both for the total cross section and for distributions.

In previous works [7] the same partonic process $us \rightarrow cdW^+W^-$ has been used for EVBA vs exact comparisons at fixed energy. For this reason we have tried to reproduce the results of [7], using as closely as possible the same cuts and parameters. On one side, this represented a test of our implementation of EVBA and, on the other side, it allowed us to determine whether the EVBA results are improved by this new and more rigorous formulation. We have computed the total cross section at a fixed center-of-mass energy of 1 TeV in the limit of infinite Higgs mass and with Higgs masses $M_h = 130, 250, 500$ GeV. In Table III the cross sections and corresponding ratios are reported. We have also compared a number of distributions obtained with the two versions of EVBA and with the exact calculation. Our more sophisticated implementation does not appear to improve substantially the agreement with the exact results.

Finally, we have analyzed the sensitivity of the results to the angular cut in the $M_h = 500$ GeV Higgs case. The total cross sections for $\theta_{\text{cut}} = 10^\circ, 30^\circ, 60^\circ$ are presented in Table IV which shows that the EVBA is more sensitive to the angular cut than the exact computation. The corresponding $M(WW)$ distribution is shown in Fig. 5. We see that the relationship between the exact and EVBA results

TABLE III. Total cross sections computed with EVBA and exact computation and their ratios for the process $us \rightarrow cdW^+W^-$ at fixed CM energy $\sqrt{s} = 1$ TeV.

M_h	EVBA (pb)	Exact (pb)	Ratio
∞	3.90×10^{-2}	1.78×10^{-2}	2.17
130 GeV	3.94×10^{-2}	1.71×10^{-2}	2.3
250 GeV	4.61×10^{-2}	4.09×10^{-2}	1.12
500 GeV	4.42×10^{-2}	2.5×10^{-2}	1.77

TABLE IV. Total cross section in EVBA and exact computation and their ratios for different angular cuts. The CM energy is $\sqrt{s} = 1$ TeV and the Higgs mass is $M_h = 500$ GeV.

θ_{cut}	EVBA (pb)	Exact (pb)	Ratio
10°	4.42×10^{-2}	2.5×10^{-2}	1.77
30°	1.33×10^{-2}	2.06×10^{-2}	0.64
60°	6.06×10^{-3}	1.28×10^{-2}	0.47

depends quite appreciably on the angular cut. The EVBA overestimates the exact result at $\theta_{\text{cut}} = 10^\circ$ by about a factor of 2 outside the Higgs peak, while the two distributions are in fair agreement at the resonance. However, the EVBA underestimates the correct result at $\theta_{\text{cut}} = 60^\circ$ over the whole mass range. The difference decreases from about a factor of 2 at small invariant masses to roughly 20% at masses larger than the Higgs mass. Therefore, while it appears quite possible to find a set of cuts, at fixed energy and Higgs mass, for which the EVBA approximation re-

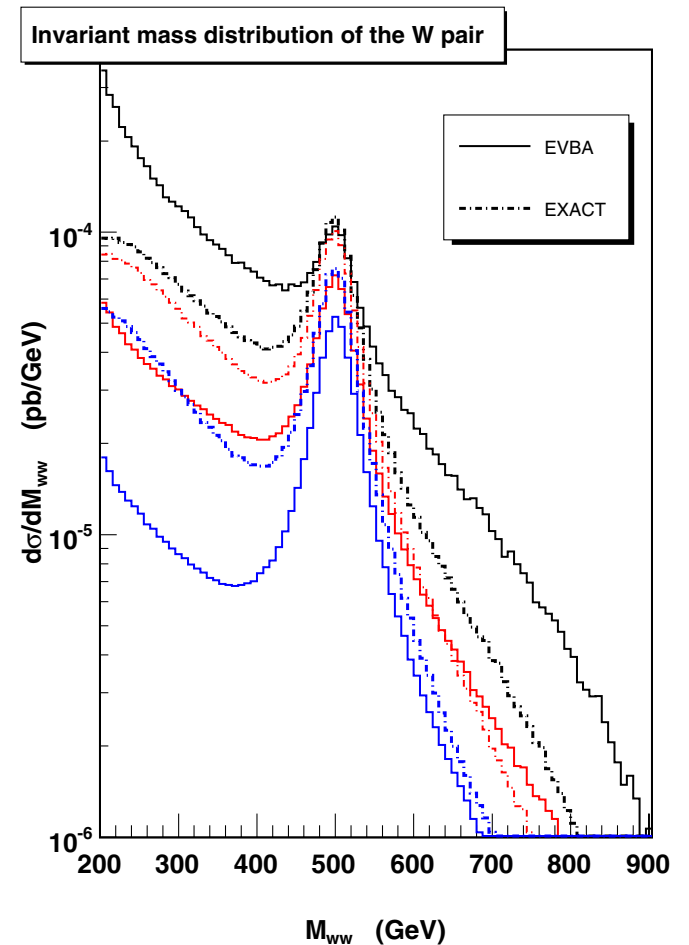


FIG. 5 (color online). The WW invariant mass distribution with different θ cuts with EVBA (solid curves) and with the exact calculation (dashed curves). From top to bottom, $\theta_c = 10^\circ$ (black), 30° (red), 60° (blue). The CM energy is $\sqrt{s} = 1$ TeV and $M_h = 500$ GeV.

produces well the exact result for the total cross section, in general it is extremely difficult to extract from the EVBA more than a very rough estimate of the actual behavior of the standard model predictions for boson-boson scattering.

VI. THE LARGE INVARIANT MASS REGION

The results presented in Secs. II and V lead to the conclusion that the boson-boson subamplitude cannot reliably be extracted from the full $qq \rightarrow qqVV$ amplitude. However the full amplitude is sensitive to the details of the EWSB mechanism. If no light Higgs is present in the SM spectrum, some hitherto unknown mechanism must intervene to enforce unitarity of the S matrix which embodies the conservation of total probability. The infinite Higgs mass limit violates perturbative unitarity in on-shell boson-boson scattering but, on the other hand, can be computed exactly, while the many available models for unitarizing the theory deal exclusively with on-shell bosons and can only approximately be incorporated in a description of $qq \rightarrow qqVV$ processes or in a six final state fermion framework, which has recently become available for the LHC [23,24].

At the LHC the linear rise of the cross section at large boson-boson invariant masses squared entailed by the leading behavior of boson-boson scattering in the SM with a very large Higgs mass will be overcome by the decrease of the parton luminosities at large x and will be particularly challenging to detect. In the absence of a more reliable theory we have adopted the no-Higgs model as a poor man's substitute.

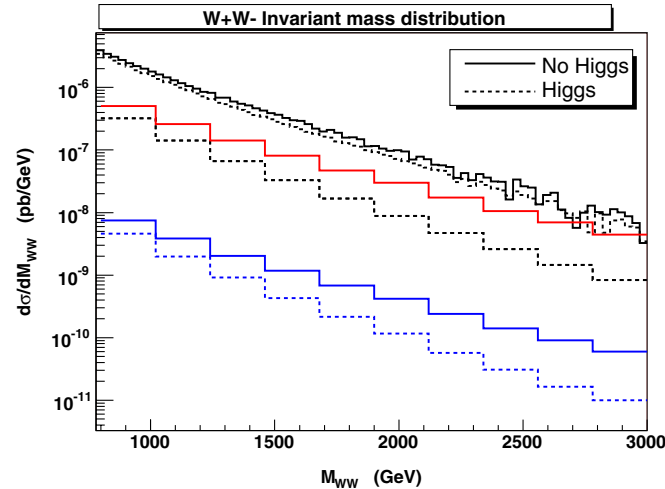


FIG. 6 (color online). The WW invariant mass distribution in $PP \rightarrow us \rightarrow cdW^+W^-$ at the LHC for the infinite Higgs mass case (solid lines) and for $M_h = 200$ GeV (dashed lines). The two intermediate (red) lines have been obtained imposing the set of cuts described in the text. The two lowest (blue) lines refer to the process $PP \rightarrow us \rightarrow cd\mu^- \bar{\nu}_\mu e^+ \nu_e$; in this case further acceptance cuts have been imposed on the charged leptons: $E_l > 20$ GeV, $p_{T_l} > 10$ GeV, $|\eta_l| < 3$.

TABLE V. Selection cuts applied in Fig. 6.

$E(\text{quarks}) > 20$ GeV
$p_T(\text{quarks}, W) > 10$ GeV
$2 < \eta(\text{quark}) < 6.5$
$ \eta(W) < 3$

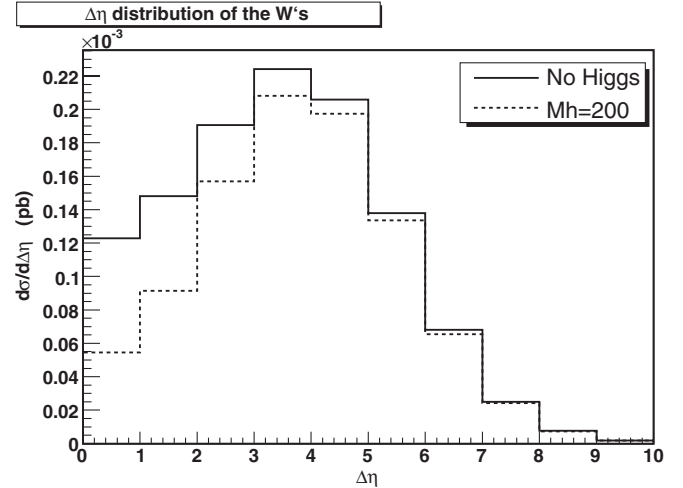


FIG. 7. Distribution of the pseudorapidity difference between the two W 's for $us \rightarrow dcW^+W^-$ at the LHC for the infinite Higgs mass case (solid line) and $M_h = 200$ GeV (dashed line).

In Fig. 6 we show the large mass tail of the boson pair invariant mass distribution for the no-Higgs case and for a Higgs mass of 200 GeV. In the absence of cuts the two results differ by about 20% over the full range. With appropriate cuts the difference between the two cases can be significantly increased. Applying the selection cuts in Table V we obtain the two intermediate (red) lines in Fig. 6. The two lowest (blue) lines refer to the full process $PP \rightarrow us \rightarrow cd\mu^- \bar{\nu}_\mu e^+ \nu_e$; in this case further acceptance cuts have been imposed on the charged leptons: $E_l > 20$ GeV, $p_{T_l} > 10$ GeV, $|\eta_l| < 3$. We see that the separation between the two Higgs mass hypotheses persists also in this more realistic setting.

As an example of the different kinematical distributions in the two cases, we show in Fig. 7 the absolute value of the difference between the pseudorapidities of the two W 's. It is interesting that the shape of the kinematical distributions, which are less sensitive to pdf uncertainties than their absolute normalization, behaves differently when a light Higgs is present in the spectrum than when its mass is very large. For more details we refer to [25,26]. We conclude that, while it does not appear to be possible to study the contribution of the scattering diagrams in isolation from the remaining ones, the full amplitude, in the region of large WW invariant masses at LHC energies, is sensitive to the presence of a light Higgs and therefore to the details of the mechanism of EWSB.

VII. CONCLUSIONS

We have critically examined the role of gauge invariance in VV fusion processes and the reliability of the EVBA in describing them in the unitary, Feynman, and axial gauges. We have shown that the WW scattering diagrams do not constitute the dominant contribution in any phase space region for the set of gauge fixing we have examined. The axial gauge as proposed in [12] results in less severe cancellations between the contribution of nonscattering diagrams and the contribution of the WW scattering ones, but typically the two sets have comparable magnitude.

We have shown that EVBA results and their relationship to exact results depend quite sensitively on the set of cuts which need to be applied in order to obtain a finite result. Therefore, it is extremely difficult to extract from the EVBA more than a very rough estimate of the actual behavior of the standard model predictions for boson-boson scattering.

We conclude that, while it seems impossible to isolate the contribution of the scattering diagrams, the mechanism of EWSB can be investigated, using the full amplitude, by a careful analysis of the region of large WW invariant masses at the LHC.

ACKNOWLEDGMENTS

E. A. is supported by the Italian Ministero dell'Istruzione, dell'Università e della Ricerca (MIUR) under Contract Decreto MIUR 26-01-2001 N.13 "Incentivazione alla mobilità di studiosi stranieri ed italiani residenti all'estero." This work is supported by MIUR under Contract No. 2004021808_009.

APPENDIX: AXIAL GAUGE

We report here for convenience the main formulas describing the axial gauge formulation of [12] to which we refer the reader for a more detailed discussion. Parametrizing the Higgs field as

$$\phi(x) = \left(\begin{array}{c} iw(x) \\ \sqrt{\frac{1}{2}}[\nu + h(x) + iz(x)] \end{array} \right).$$

the propagator for the five dimensional vector field (W^μ, w) is

$$i\Delta^{IJ} = \frac{i}{q^2 - M_W^2} N^{IJ}(q) \quad (\text{A1})$$

where

$$N^{\mu\nu}(q) = -g^{\mu\nu} + \frac{q^\mu n^\nu + n^\mu q^\nu}{q \cdot n} - \frac{n^2}{(q \cdot n)^2} q^\mu q^\nu, \quad (\text{A2})$$

$$N^{\mu s}(q) = -iM_W \frac{q \cdot n n^\mu + n^2 q^\mu}{(q \cdot n)^2}, \quad (\text{A3})$$

$$N^{s\nu}(q) = N^{\nu s}(q)^* = N^{\nu s}(-q), \quad (\text{A4})$$

$$N^{ss}(q) = 1 - \frac{M_W^2 n^2}{(q \cdot n)^2}, \quad (\text{A5})$$

and the index s indicates the scalar component.

The polarization vectors satisfy

$$N^{IJ}(q) = \sum_{\lambda=1,2,L} \epsilon^I(q, \lambda) \epsilon^J(q, \lambda)^*. \quad (\text{A6})$$

For $\lambda = 1, 2$ they describe transverse polarization,

$$\begin{aligned} \epsilon^s(q, \lambda) &= 0, & q_\mu \epsilon^\mu(q, \lambda) &= 0, & n_\mu \epsilon^\mu(q, \lambda) &= 0, \\ \epsilon_\mu(q, \lambda) \epsilon^\mu(q, \lambda')^* &= -\delta_{\lambda\lambda'}, \end{aligned} \quad (\text{A7})$$

while for $\lambda = L$ they describe longitudinal polarization,

$$\epsilon^s(q, L) = -i\sqrt{1 - M_W^2 n^2 / (q \cdot n)^2}, \quad (\text{A8})$$

$$\epsilon^\mu(q, L) = \frac{-[M_W/q \cdot n]n^\mu + [M_W^2 n^2 / (q \cdot n)^2]q^\mu}{\sqrt{1 - M_W^2 n^2 / (q \cdot n)^2}}. \quad (\text{A9})$$

The propagators and polarizations for the (Z^μ, w) field can be obtained from Eqs. (A1)–(A9) with the substitution $M_W \rightarrow M_Z$.

The remaining Feynman rules are identical to the ones in R_ξ gauges. In our calculation we have used $\xi = 1$.

-
- [1] ATLAS, Report No. CERN-LHCC-99-14 and No. CERN-LHCC-99-1.
 [2] K. A. Assamagan *et al.* (Higgs Working Group), hep-ph/0406152.
 [3] A. Djouadi, hep-ph/0503172.
 [4] M. S. Chanowitz, hep-ph/9812215.
 [5] M. J. Duncan, G. L. Kane, and W. W. Repko, Nucl. Phys. **B272**, 517 (1986).

- [6] D. A. Dicus and R. Vega, Phys. Rev. Lett. **57**, 1110 (1986).
 [7] J. F. Gunion, J. Kalinowski, and A. Tofighi-Niaki, Phys. Rev. Lett. **57**, 2351 (1986).
 [8] S. Dawson, Nucl. Phys. **B249**, 42 (1985).
 [9] G. L. Kane, W. W. Repko, and W. B. Rolnick, Phys. Lett. **148B**, 367 (1984).
 [10] J. Lindfors, Z. Phys. C **28**, 427 (1985).

- [11] R. Kleiss and W.J. Stirling, *Phys. Lett. B* **182**, 75 (1986).
- [12] Z. Kunszt and D.E. Soper, *Nucl. Phys.* **B296**, 253 (1988).
- [13] E. Accomando, hep-ph/0604273.
- [14] R.N. Cahn, *Nucl. Phys.* **B255**, 341 (1985).
- [15] S.S.D. Willenbrock and D.A. Dicus, *Phys. Rev. D* **34**, 155 (1986).
- [16] C.F. von Weizsäcker, *Z. Phys.* **88**, 612 (1934).
- [17] E.J. Williams, *Phys. Rev.* **45**, 729 (1934).
- [18] R.N. Cahn and S. Dawson, *Phys. Lett.* **136B**, 196 (1984).
- [19] M.S. Chanowitz and M.K. Gaillard, *Phys. Lett.* **142B**, 85 (1984).
- [20] R.M. Godbole and F.I. Olness, *Int. J. Mod. Phys. A* **2**, 1025 (1987).
- [21] I. Kuss and H. Spiesberger, *Phys. Rev. D* **53**, 6078 (1996).
- [22] P.W. Johnson, F.I. Olness, and W.-K. Tung, *Phys. Rev. D* **36**, 291 (1987).
- [23] E. Accomando, A. Ballestrero, and E. Maina, *J. High Energy Phys.* 07 (2005) 016.
- [24] A. Ballestrero, A. Belhouari, G. Bevilacqua, and E. Maina (unpublished).
- [25] E. Accomando, A. Ballestrero, S. Bolognesi, E. Maina, and C. Mariotti, *J. High Energy Phys.* 03 (2006) 093.
- [26] E. Accomando, A. Ballestrero, A. Belhouari, and E. Maina, hep-ph/0603167.